Supplemental Information for Mesoscale Interplay Between Phonons and Crystal Electric Field Excitations in Quantum Spin Liquid Candidate $CsYbSe_2$

1. TEMPERATURE DEPENDENCE FOR HIGHER ENERGY BAND

Figure S1 shows temperature-dependent unpolarized Raman spectra taken in a higher energy band from $T = 3.3$ K to $T = 270$ K. The spectra were taken with Semrock dichroic and longpass filters instead of a set of volume Bragg gratings.

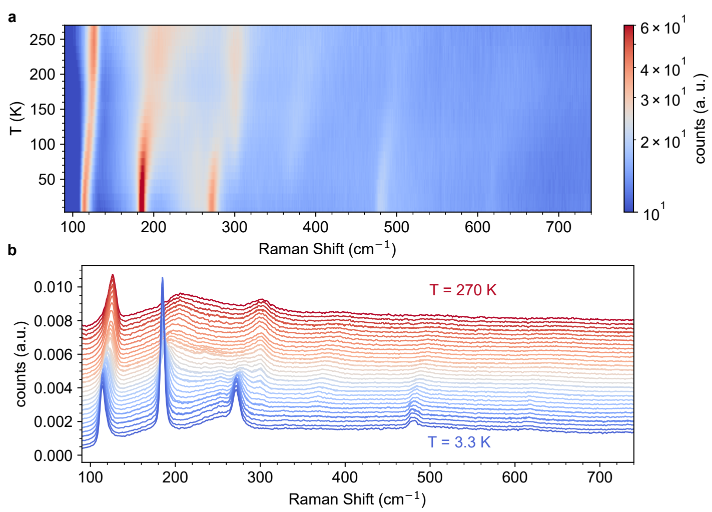

Fig. S1. Raman spectra in a higher energy band as a function of temperature from $T = 3.3$ K to $T = 270$ K.

2. RAMAN GROUP THEORY ANALYSIS FOR CSYBSE$_2$

$CsYbSe_2$ belongs to the space group $P6_3/mmc$ (No. 194) with the point group D_{6h}, and its Raman active phonon modes consist of non-degenerate A_{1g} symmetry modes, doubly degenerate E_{2g} symmetry modes ($E_{2g}-x$ and $E_{2g}-y$), and doubly degenerate E_{1g} symmetry modes ($E_{1g}-x$ and $E_{1g}-y$). Their Raman tensors $\widetilde{R}$ assume the following forms:

$$\widetilde{R}(A_{1g}) = \begin{pmatrix} a & \cdot & \cdot \\ \cdot & a & \cdot \\ \cdot & \cdot & b \end{pmatrix}$$

$$\widetilde{R}(E_{2g}-x) = \begin{pmatrix} c & \cdot & \cdot \\ \cdot & -c & \cdot \\ \cdot & \cdot & \cdot \end{pmatrix}; \widetilde{R}(E_{2g}-y) = \begin{pmatrix} \cdot & c & \cdot \\ c & \cdot & \cdot \\ \cdot & \cdot & \cdot \end{pmatrix}$$

$$\widetilde{R}(E_{1g}-x) = \begin{pmatrix} \cdot & \cdot & \cdot \\ \cdot & \cdot & d \\ \cdot & d & \cdot \end{pmatrix}; \widetilde{R}(E_{1g}-y) = \begin{pmatrix} \cdot & \cdot & d \\ \cdot & \cdot & \cdot \\ d & \cdot & \cdot \end{pmatrix} \tag{S1}$$

In the experimental back-scattering laser geometry (light Z in and Z out) with linear polarization, the electric polarization vectors of the scattered and incident light $\mathbf{e}_s$ and $\mathbf{e}_i$ are in-plane (i.e., the X-Y plane), and they are given by $\mathbf{e}_s$ = (cosγ, sinγ, 0) and $\mathbf{e}_i$ = (cosθ, sinθ, 0). With Raman intensity $I \propto |\mathbf{e}_s \cdot \widetilde{R} \cdot \mathbf{e}_i^T|^2$, we have:

$$I \propto \left| \begin{pmatrix} cos\gamma, & sin\gamma, & 0 \end{pmatrix} \cdot \widetilde{R} \cdot \begin{pmatrix} cos\theta \\ sin\theta \\ 0 \end{pmatrix} \right|^2 \tag{S2}$$

It is obvious that E_{1g} phonon modes have zero Raman intensity in the back-scattering geometry, and thus cannot be observed experimentally. For A_{1g} and E_{2g} modes, by substituting the Raman tensors $\widetilde{R}$ from Eq. S1 into Eq. S2, we can obtain

$$\begin{aligned} I(A_{1g}) &\propto \left| \begin{pmatrix} cos\gamma, & sin\gamma, & 0 \end{pmatrix} \cdot \begin{pmatrix} a & \cdot & \cdot \\ \cdot & a & \cdot \\ \cdot & \cdot & b \end{pmatrix} \cdot \begin{pmatrix} cos\theta \\ sin\theta \\ 0 \end{pmatrix} \right|^2 \\ &\propto |acos\gamma cos\theta + asin\gamma sin\theta|^2 \\ &\propto |a|^2 cos^2(\gamma - \theta) \end{aligned} \tag{S3}$$

$$\begin{aligned} I(E_{2g}-x) &\propto \left| \begin{pmatrix} cos\gamma, & sin\gamma, & 0 \end{pmatrix} \cdot \begin{pmatrix} c & \cdot & \cdot \\ \cdot & -c & \cdot \\ \cdot & \cdot & \cdot \end{pmatrix} \cdot \begin{pmatrix} cos\theta \\ sin\theta \\ 0 \end{pmatrix} \right|^2 \\ &\propto \left| \begin{pmatrix} ccos\gamma, & -csin\gamma, & 0 \end{pmatrix} \cdot \begin{pmatrix} cos\theta \\ sin\theta \\ 0 \end{pmatrix} \right|^2 \\ &\propto |ccos\gamma cos\theta - csin\gamma sin\theta|^2 \\ &\propto |c|^2 cos^2(\gamma + \theta) \end{aligned} \tag{S4}$$

$$
\begin{aligned}
I(\mathrm{E_{2g}}-y) &\propto \left| \begin{pmatrix} cos\gamma, & sin\gamma, & 0 \end{pmatrix} \cdot \begin{pmatrix} \cdot & c & \cdot \\ c & \cdot & \cdot \\ \cdot & \cdot & \cdot \end{pmatrix} \cdot \begin{pmatrix} cos\theta \\ sin\theta \\ 0 \end{pmatrix} \right|^2 \\
&\propto \left| \begin{pmatrix} csin\gamma, & ccos\gamma, & 0 \end{pmatrix} \cdot \begin{pmatrix} cos\theta \\ sin\theta \\ 0 \end{pmatrix} \right|^2 \\
&\propto |csin\gamma cos\theta + ccos\gamma sin\theta|^2 \\
&\propto |c|^2 sin^2(\gamma+\theta)
\end{aligned}
\tag{S5}
$$

Consequently, the Raman intensity of a doubly degenerate $\mathrm{E_{2g}}$ mode is

$$
I(\mathrm{E_{2g}}) = I(\mathrm{E_{2g}}-x) + I(\mathrm{E_{2g}}-y) = |c|^2 cos^2(\gamma+\theta) + |c|^2 sin^2(\gamma+\theta) = |c|^2 \tag{S6}
$$

Eq. S6 indicates that the polarization profile of an $\mathrm{E_{2g}}$ phonon mode is a circle under any linear polarization configuration. For an $\mathrm{A_{1g}}$ phonon mode, under the experimental parallel polarization configuration (i.e., XX, $\gamma = \theta$), its intensity I($\mathrm{A_{1g}}$) $\propto |a|^2$ according to Eq. S3 and hence the polarization profile is also a circle; however, under the experimental cross polarization configuration (i.e., XY, $\gamma = \theta + 90°$), its intensity I($\mathrm{A_{1g}}$) = 0. These results are in agreement with the experimental data. Interestingly, the polarization profiles of CEFs Raman modes are very similar to the polarization profiles of $\mathrm{E_{2g}}$ phonon modes, suggesting that CEFs modes share similar forms of Raman tensors to $\mathrm{E_{2g}}$ phonon modes.

3. POLARIZATION AND ANGULAR DEPENDENCE

Figure S2 shows the polarization dependence of the peaks $\mathrm{E_{2g}^1}$, CEF1, CEF2 and CEF3 $T = 3.3$ K, $\mathrm{E_{2g}^1}$, $\mathrm{E_{2g}^2}$ and $\mathrm{A_{1g}}$ at $T = 293$ K.

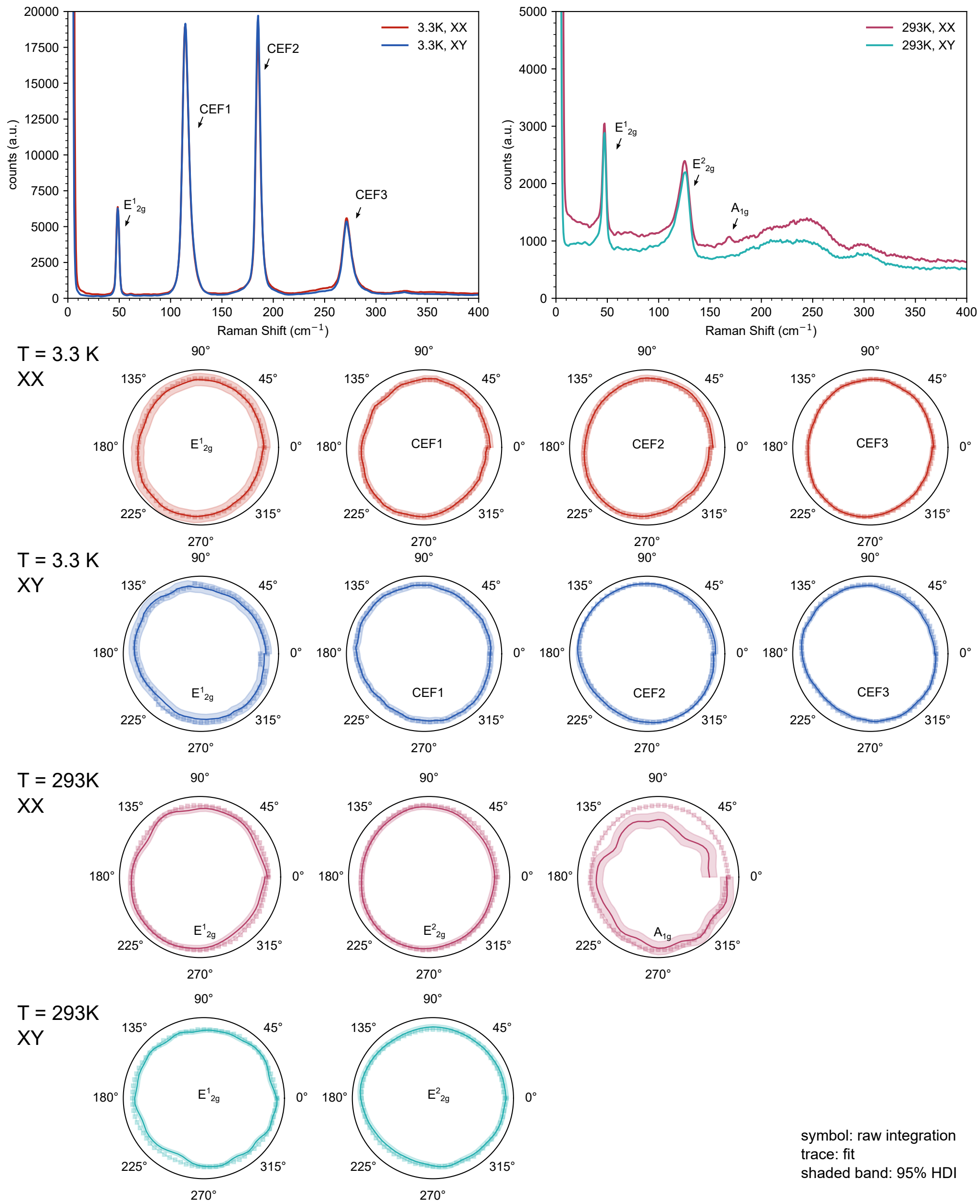

Fig. S2. Polarization and angular dependence of the at $T = 3.3$ K and $T = 293$ K.

4. CALCULATED PHONON DISPERSION

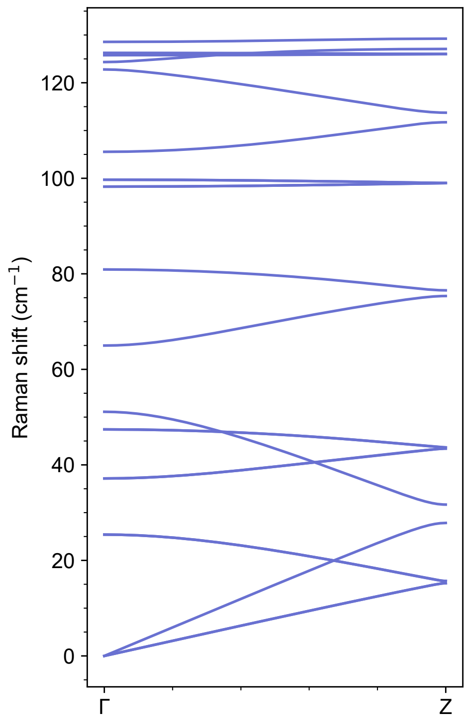

Fig. S3. Calculated phonon dispersion

5. POSITION DEPENDENCE

As described in the main text, we report subtle spatial anti-correlations between phonon and CEF modes, such as the CEF1, E_{2g}^2, and ω_2 modes. Simple spatial plots of integrated counts over a specific peak may be affected by baseline corrections and/or large peaks nearby. The baseline can be removed by asymmetric least squares fitting but the accuracy is not necessarily satisfactory. Meanwhile, full-blown curve fitting over thousands of spatial points can be computational expensive. Non-negative matrix factorization (NMF) is a simple algorithm that captures the most linearly independent basis vectors out of a given hyper-dimensional data cube with very low computational cost, yet it is effective in exploratory data analysis. Here Figures S4, S5, and S6 illustrate spatially resolved Raman spectra at $T = 3$ K, $T = 120$ K, and $T = 130$ K, respectively. In these figures, (a) illustrates a subset of raw Raman spectra, with the inset illustrating the captured NMF components. (b-e) are integrated counts for selected peaks. (f-h) are the weights with respect to the basis vector components for the NMF decomposition. A similar anticorrelation between modes to that described in the main text is observed again in these representations. The (x, y) are the raw coordinate values. A value of $(x, y) = (2127\ \mu\text{m}, 104\ \mu\text{m})$ was subtracted in the main text.

A. T = 3K

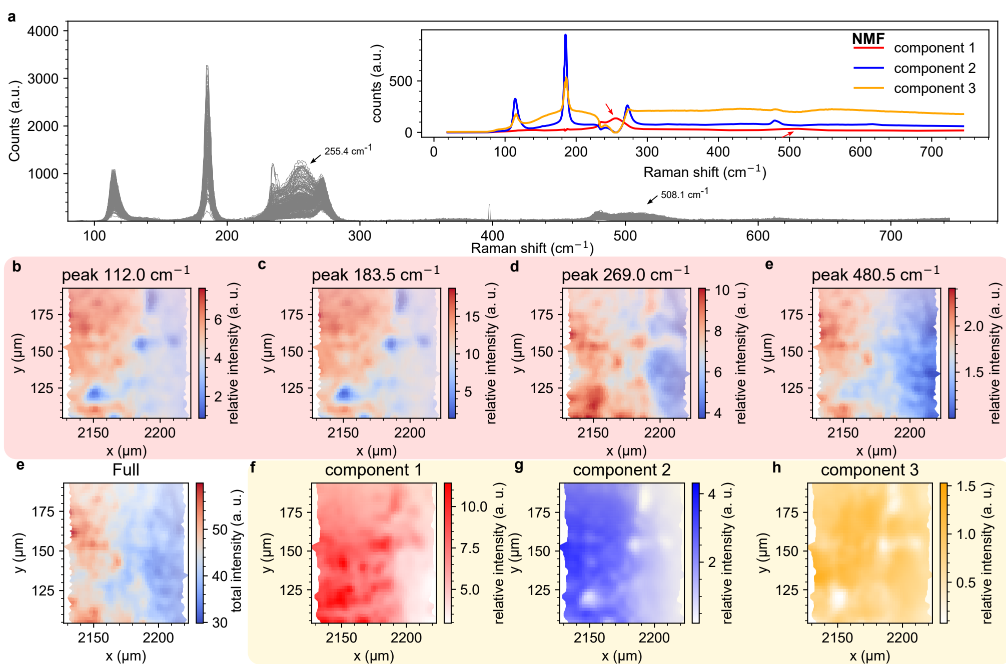

Fig. S4. Position Dependence at $T = 3.3$ K.

B. T = 120K

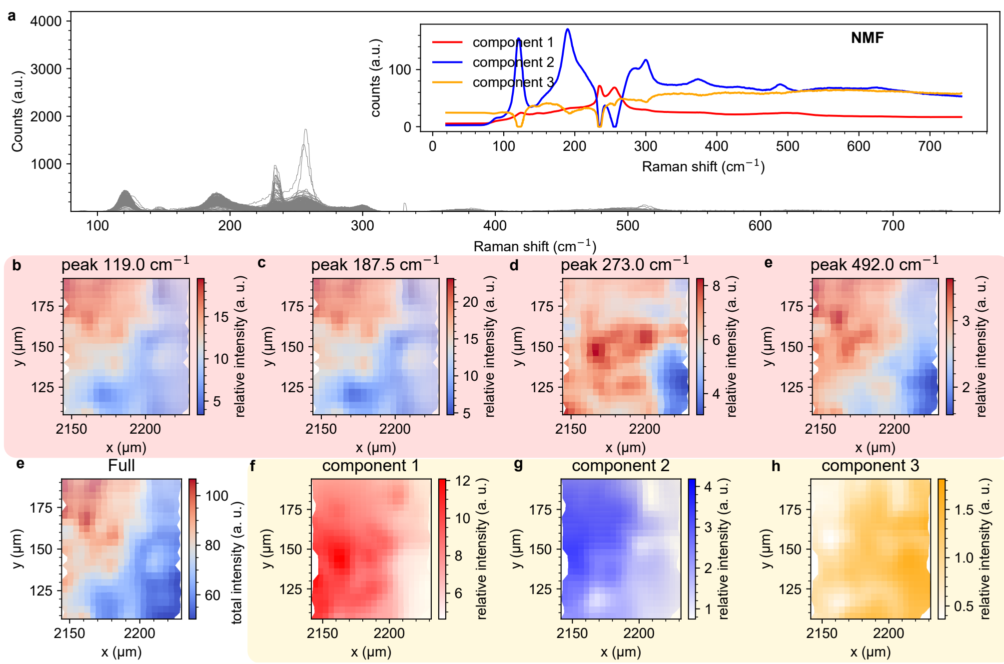

Fig. S5. Position Dependence at T = 120 K.

C. T = 130K

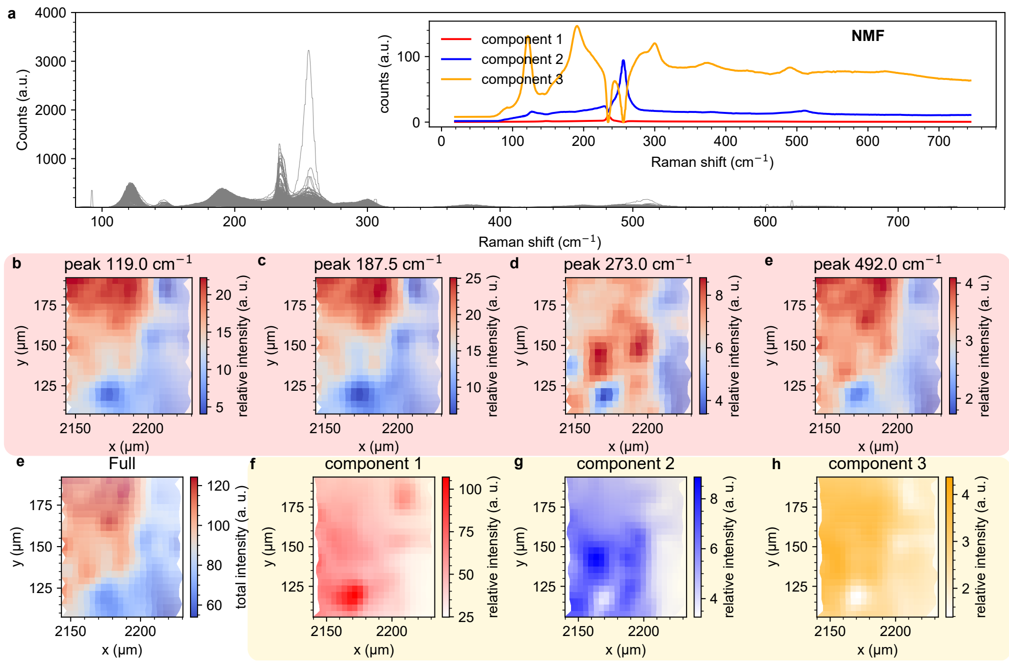

Fig. S6. Position Dependence at T = 130 K.